Stimulated Emission Depletion Microscopy

8

Silvia Galiani, Jana Koth, Ulrike Schulze,
and B. Christoffer Lagerholm

Contents

What You Will Learn in This Chapter

Stimulated emission depletion (STED) microscopy is in its simplest form an extension of confocal fluorescence microscopy that offers much enhanced spatial resolution in both 2D and 3D. This chapter provides a basic overview of the theory behind STED microscopy and the technology developments and modern design of the STED microscope. Like with any advanced imaging technology, it is important to implement simple testing procedures of the overall performance. This chapter

S. Galiani · U. Schulze
Wolfson Imaging Centre Oxford, MRC Weatherall Institute of Molecular Medicine, University of Oxford, Headley Way, Oxford, UK

MRC Human Immunology Unit, MRC Weatherall Institute of Molecular Medicine, University of Oxford, Headley Way, Oxford, UK

J. Koth · B. Christoffer Lagerholm (✉)
Wolfson Imaging Centre Oxford, MRC Weatherall Institute of Molecular Medicine, University of Oxford, Headley Way, Oxford, UK
e-mail: christoffer.lagerholm@imm.ox.ac.uk

V. Nechyporuk-Zloy (ed.), *Principles of Light Microscopy: From Basic to Advanced*, https://doi.org/10.1007/978-3-031-04477-9_8

provides detailed examples of the testing procedures that have proven useful to ensure optimal performance of a range of STED microscopes. Finally, this chapter includes a few application image examples.

8.1 Introduction

STED (stimulated emission depletion) microscopy is a far-field super-resolution fluorescence microscopy technique that allows fluorescence imaging with, in principle, unlimited spatial resolution. The concept of STED microscopy was first introduced in 1994 [1], and the first successful experimental implementation of STED microscopy applied to a biological specimen was published in 2000 [2]. STED microscopy has subsequently become a well-established super-resolution microscopy technique suitable for imaging a broad range of biological samples with a resolution that is much smaller than the conventional diffraction-limited resolution that can be obtained by a conventional confocal microscope. STED microscopy can further be efficiently combined with fluorescence correlation spectroscopy (FCS), thus enabling super-resolution studies of, for example, diffusion in cell membranes [3, 4]. The implementation of STED-FCS, which follows the same general approach as for conventional FCS, has the unique ability to enable studies at observation volumes much smaller than the diffraction limit. For further details on implementation and practical guide to STED-FCS, we refer the reader to Sezgin et al. [5].

8.2 Basic Principle of the STED Microscope

STED microscopy enables imaging beyond the diffraction limit by exploiting the property that there are two distinct relaxation routes: (1) spontaneous emission, and (2) stimulated emission, whereby an excited fluorescent molecule can return to the ground state. This is illustrated in terms of a Jablonski diagram in Fig. 8.1a. In STED microscopy, as is the case for conventional confocal microscopy, photons from the excitation laser are absorbed by fluorophores in the specimen resulting in a molecular transition to a higher excited state. In the case of conventional confocal microscopy, subsequent to internal conversion, the excited molecules would ideally return, with a high yield, to the ground state via “spontaneous emission” whereby photons of light, red-shifted relative to the excitation wavelength, are emitted and detected as conventional fluorescence. In the case of STED microscopy, however, a significant fraction of excited molecules, as defined by the shape of the STED point spread function (PSF), is instead stimulated to return to the ground state by “stimulated emission” upon exposure by the STED laser. In this context, it is important to remember that relaxation by stimulated emission is not a dark process but rather is a process where relaxation to the ground state, as stimulated by the STED laser, results in the emission of a photon of identical nature (i.e., wavelength, polarization, phase) to the photon from the STED laser. Furthermore, as the photon emitted from the STED laser is not absorbed by the excited dye, this process results in an exact

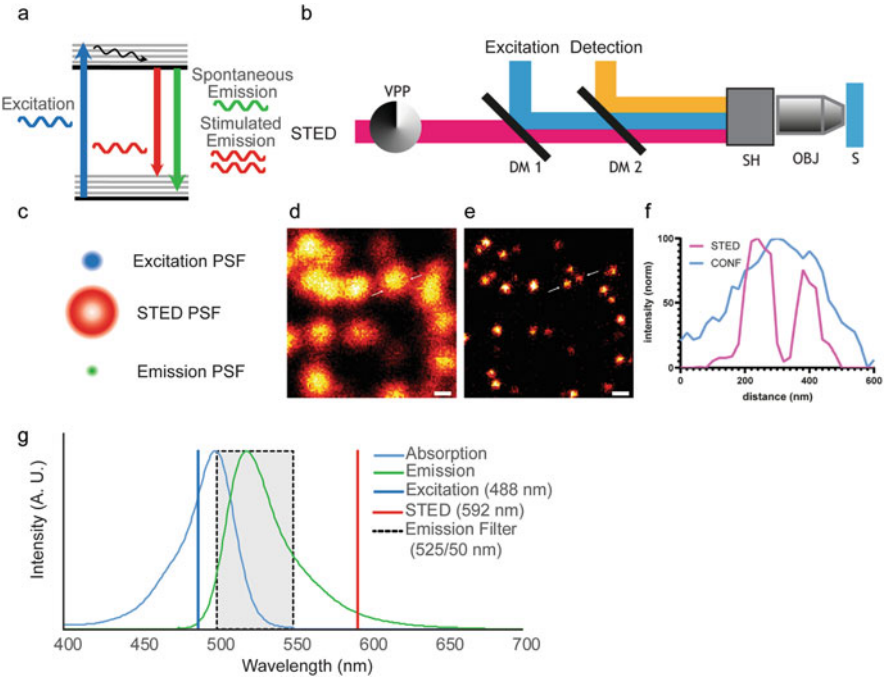

Fig. 8.1 Principles of STED microscopy. (**a**) Schematic of STED microscopy in terms of a Jablonksi diagram illustrating the transitions in electronic state during conventional fluorescence (i.e., spontaneous emission) and during stimulated emission. (**b**) Schematic of optical path of a 2D STED microscope. The excitation laser path (excitation; blue) and the STED beam (STED; pink), donut shaped via a vortex phase plate (VPP), are super-positioned in the sample plane (S) via scanning head (SH) and objective (OBJ). (**c**) Schematic of 2D cross section of excitation point-spread function (PSF)(blue), 2D-STED PSF with zero intensity at the center (red), and effective emission PSF (green) that would result from the super-position of the excitation and STED PSFs. (**d**) Example confocal and (**e**) STED image of the same field of view of fluorescent beads. Also shown in (**d**, **e**) are white arrows indicating the location of the fluorescent intensity profiles shown in f) for the confocal image (blue line) and STED image (pink line). Scale bars = 200 nm. (**g**) Schematic of STED microscopy in terms of asorption and emission spectra for sample stained with Alexa Fluor 488 showing the typical selection of the excitation laser (488 nm), the STED laser (592 nm), and the emission bandpass filter settings (525/50 nm) for sample stained with Alexa Fluor 488

doubling of the photon emitted by the STED laser. A key aspect in the design of the detection window in STED microscopy is thus to ensure that the emission bandpass filter does not overlap with the STED laser such that the photons that result from the stimulated emission process are, as far as the detector is concerned, effectively a dark state. A second key aspect in STED microscopy, and the reason for the requirement of exquisite time control, is that the STED laser is able to stimulate a vast majority of specific molecules to return to the ground state prior to the occurrence of relaxation by conventional spontaneous emission. Because most fluorophores have a mean excited state lifetime of a few nanoseconds, this introduces a requirement that the

STED depletion process must ideally occur within a fraction of a ns after the excitation process.

8.3 Basic Design of the STED Microscope

The basic layout of a STED microscope is the same as for traditional confocal microscopy with an additional requirement of the incorporation of a STED laser, optical elements that enable exquisite shaping of the STED laser beam, and electronics for exquisite control of the time synchronization of the STED laser relative to the excitation laser. A 2D STED implementation via a vortex phase mask is shown in Fig. 8.1b. The excitation path is based on a confocal optical scheme. The laser light is focused onto the sample via the objective lens, and the resulting fluorescence is collected back pixel by pixel via the same objective lens and detected via a high sensitivity point detector such as avalanche photo diodes (APDs). A pinhole aperture positioned before the detector guarantees the optical section of the sample. The shape of the STED beam is adjusted by the vortex plate, and the resulting shaped beam is spatially and temporally adjusted to closely overlap the excitation beam in the sample plan.

In the case of 2D STED, the function of the beam shaping optical elements is to engineer the point-spread function (PSF) of the STED laser to a donut pattern with a zero intensity foci in the middle (Fig. 8.1c), while any number of alternate beam shapes have also been demonstrated, including for 3D STED [6]. A prerequisite for STED microscopy is that the centroid of the conventional diffraction-limited PSF of the excitation laser (Fig. 8.1c) is perfectly co-aligned in space with the centroid of the PSF of the STED laser, and furthermore that the arrival time of the excitation laser and STED laser at the sample plane is precisely controlled. With such exquisite spatial and temporal control, it is possible to create an effective emission PSF (or observation volume; Fig. 8.1c) that is much smaller than the conventional diffraction limit. With such a STED microscope, it is possible to acquire both a conventional confocal image of e.g. fluorescent beads with an inactive STED laser beam at conventional diffraction-limited resolution (Fig. 8.1d) and a super-resolution STED image of the same specimen with an active STED laser beam with a much improved resolution (Fig. 8.1e) as is clearly demonstrated by the representative example of fluorescence intensity line profile in Fig. 8.1f.

An important characteristic of STED microscopy is also that it is possible to tune the resolution of the STED microscope by adjusting the STED laser power. As a result, the diffraction barrier no longer limits the resolution of a STED microscope that increases with increasing intensity of the STED laser:

$$d_{\mathrm{STED}} = \frac{d}{\sqrt{1 + A\frac{I_{\mathrm{STED}}}{I_S}}} \tag{8.1}$$

where d is the diameter of the diffraction-limited excitation laser spot, $A > 0$ is a geometrical parameter that takes into account the shape of the STED laser beam, I_{STED} is the STED laser intensity, and I_S is the so-called saturation intensity, characteristic for a specific fluorescence label representing how efficiently it can be depleted. To increase the lateral resolution of a standard confocal microscope a donut-shaped STED beam is generated via a vortex phase mask; to increase the axial resolution of a standard confocal microscope a bottleneck STED beam is created via a pi phase mask. A combination of both masks will allow tuning the resolution in both lateral and axial direction. While theoretically, the spatial resolution can be pushed to unlimited scales, the signal-to-noise ratio is a limiting factor. In practice, this means that a typical resolution up to about 50 nm can be routinely achieved for cell studies.

In order to answer to the multiple demands coming from biological and biomedical applications, the most common implementation is a multicolor STED microscope. Such a microscope allows combining different fluorescent markers in order to disclose morphology, proximity, and co-localization of molecules at a nanoscale level. A schematic of single-color STED microscopy in terms of the absorption and emission spectra of the representative green fluorophore Alexa Fluor 488 is shown in Fig. 8.1g. In STED microscopy, just as in the case of conventional confocal microscopy, the excitation laser is selected to match closely to the peak of the absorption spectra, while the emission bandpass filter is typically selected to collect emitted light broadly around the peak of the emission spectra. Meanwhile, the selection of the STED laser, typically 592 nm for green dyes, is dictated by a requirement that the laser wavelength is red-shifted relative to the peak fluorescence emission (and the emission bandpass filter) of the specific probe. These same characteristics are representative for STED microscopy of e.g. intermediate red dyes such as Alexa Fluor 555 or TMR, which can be used for STED microscopy with a 660 nm STED laser, or more red-shifted dyes such as Alexa Fluor 594, Atto 590, Abberior Star Red, or Abberior Star 635P, which can be used for STED microscopy with a 775 nm STED laser. While different excitation and STED beams could be combined to obtain a multicolor STED image, the most reliable implementation for co-localization studies employs a single STED beam to deplete multiple excitations, so that the alignment of the distinct color channels is determined by the center of the STED PSF.

8.4 Microscope Performance Tests

To ensure the best performance of a STED microscope, it is absolutely essential to check for laser stability, point spread function (PSF) distribution of excitation and STED beams, and the co-alignment of the excitation and STED laser beams. Here, we suggest a maintenance routine to guarantee reliable and comparable STED measurements. In order to follow the presented routine it is useful to be equipped with a power meter to check the stability of the STED laser, a gold bead sample to

check the alignment of the excitation and STED PSF of the beams, and a fluorescent bead sample to check alignment and resolution with fluorescence detection.

8.4.1 Laser Power Measurements

Since the STED resolution depends on the STED laser intensity power, the STED laser source needs to remain stable over time. A daily or even hourly variation of the STED power will provide different resolution effects on same dyes and so incomparable images that will nullify any data analysis. It is good practice to check weekly the laser power provided by the STED beam at different intensity levels. This measurement can be done via a power meter detector positioned on top or at the back aperture of the objective lens used to run the experiment. For these measurements, we regularly use a power sensor with a spectral range of 400–1100 nm and a maximum power rating of 500 mW (Thorlabs; S130C) and a power meter (Thorlab; PM100D). We typically measure laser powers at least every week in order to verify laser coupling stability. Different laser intensity levels can be set via software and the corresponding power recorded. A variation of more than 10% has to be considered as a possible cause for inconsistent data.

8.4.2 Gold Beads

In order to obtain a reliable STED effect, the alignment of both the excitation and STED PSF should be symmetric and straight along all directions. Such PSFs can be visualized via imaging of gold beads in reflection mode. The excitation beam should show a classical diffraction-limited point spread function (PSF) characterized by Gaussian distribution along lateral and axial directions. The STED beam in the absence of masks should have the very same profile as the excitation beam. Once a mask is applied, the beam must remain straight and show a characteristic zero intensity point in the center as shown in Fig. 8.2a. Uneven intensity distribution and tilt of the beam suggest that the optical path must be corrected (e.g., align phase plate with the beam, align mirrors, damaged lenses, or objective lens). Gold beads measurement allows also to check on the spatial alignment of the excitation and the STED beam; the beam should be coaxial along the xy-axis and positioned at the very same z-plane.

8.4.3 Fluorescent Beads, Nanorulers, and Immunostained Cell Samples

The fine alignment between excitation and STED beams should always subsequently be validated on fluorescent calibration samples such as fluorescent bead samples (Fig. 8.2b). In acquiring such STED images, just like for conventional confocal images, it is of course essential to strive to acquire images at high signal-to-noise

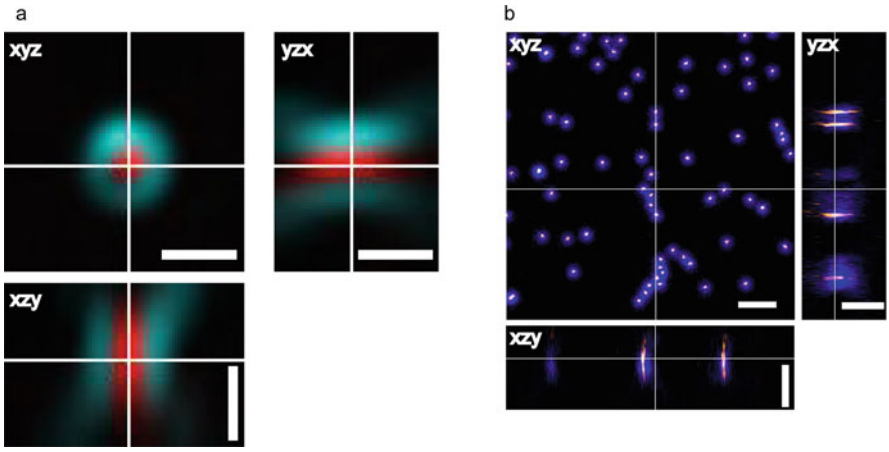

Fig. 8.2 Validation of super-position of excitation and STED beams for a well-aligned STED microscope. (**a**) Validation of spatial alignment of STED microscope with 80 nm diameter gold beads showing respectively the expected pattern of light scattered from the excitation beam (red) and the STED beam (cyan) along each axis as shown. Scale bar = 500 nm. (**b**) Validation of spatial alignment of STED microscope with fluorescent GATTA beads (GattaQuant) labeled with Atto 647 N (Bead R) showing the super-position of the confocal point-spread function (PSF; blue) and the STED PSF (orange glow) along each axis as shown. Scale bar = 1 μm

ratio (SNR) by use of either line (or frame) averaging or frame (or line) accumulation or both, and to use proper sampling according to the Nyquist theorem. In terms of sampling, this typically entails acquisition of images with a projected pixel size of at least 3× smaller than either the anticipated or determined lateral resolution. In accordance with an expected lateral resolution of around 50 nm, proper sampling would require a projected pixel size of around 15 nm.

From images of sub-diffraction-limited beads, preferably of a size of 20–40 nm in diameter, it is possible to directly visualize the effective observation volume of the STED microscope. When the highest STED laser power is applied, the maximum resolution of the microscope is measured. Tuning the STED power and combining different mask will allow an indicative calibration of the resulting observation volume. If the system is equipped with a variable pinhole aperture repeating this measurement with both a closed pinhole and an open pinhole setting allows for an evaluation of the alignment of the detection path. As a prerequisite, when the pinhole is fully opened, the STED PSF should be aligned with the excitation PSF in all directions. Upon closing the pinhole, a well-aligned STED system is characterized by a symmetric intensity distribution along the lateral direction and a straight beam along the axial direction as shown in the example in Fig. 8.2b. Furthermore, when the confocal and STED images of fluorescent beads are super-imposed, the super-resolution signal should appear in the center of the confocal image in all directions as shown in Fig. 8.2b.

Fluorescent bead samples of dimensions much smaller than the diffraction limit, usually of 20–40 nm in diameter, are also commonly used to evaluate the resolution of a STED microscope as a function of the STED laser power (Fig. 8.3). One version

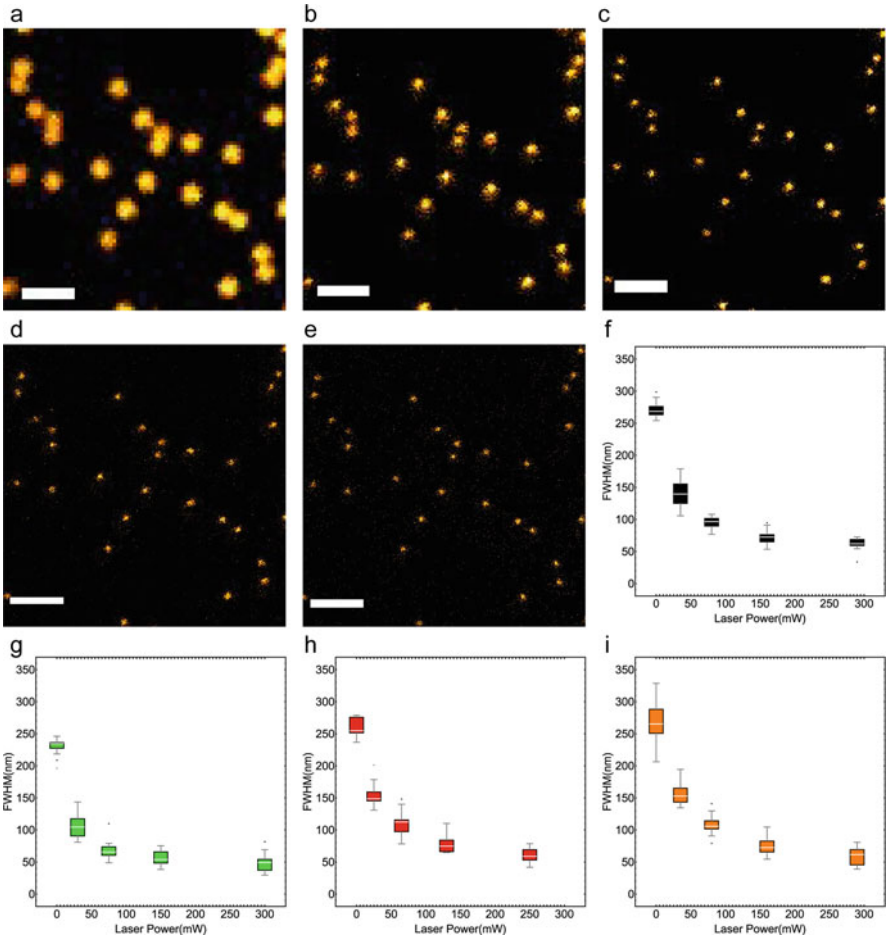

Fig. 8.3 Performance validation of STED microscope in 2D STED imaging mode with 23 nm diameter DNA origami GATTA beads (GattaQuant). (**a**–**e**) STED image examples of GATTA beads labeled with Atto647N (Bead R) that were imaged on Leica STED 3X microscope with a STED white 100X 1.40 NA Plan APO oil immersion objective, 633 nm laser excitation, a pulsed 775 nm STED laser, and time-gated detection ($0.5 \leq t_d \leq 7$ ns) with a spectral emission window of 649–701 nm. Scale bars = 1 μm. The resolution of the resulting STED images evaluated quantitatively by using the line profile tool in ImageJ (version 1.53j) to create line intensity profiles across select apparent single GATTA beads ($N = 15$ for each image condition) and by fitting the resulting line intensity profiles to one-dimensional spatial Gaussians in Wolfram Mathematica (version 12.0.0.0). (**f**) Box-and-whisker plot of FWHM values from images of GATTA beads labeled with Atto647N (Bead R). (**g**) Box-and-whisker plot of FWHM values from images of GATTA beads labeled with Oregon Green 488 (Bead B). The corresponding images were acquired on the same microscope system as for images in (**a**–**e**) except with 488 nm excitation, a CW 592 nm STED laser, and time-gated detection ($1.5 \leq t_d \leq 6.5$ ns) with a spectral emission window of 494–584 nm. (**h**) Box-and-whisker plot of FWHM values from images of GATTA beads labeled with Atto 542 (Bead G). The corresponding images were acquired on the same microscope system as for images in (**a**–**e**) except with 561 nm excitation, a CW 660 nm STED laser, and time-gated detection ($1.5 \leq t_d \leq 6.5$ ns) with a spectral emission window of 570–663 nm. i) Box-and-whisker plot of FWHM values from images of GATTA beads labeled with Atto 594 (Bead O). The corresponding images were acquired on the same microscope system as for images in (**a**–**e**) except with 561 nm excitation, a pulsed

of this uses DNA origami GATTA beads that can be ordered with the same fluorophores that are to be used in a given biological experiment. This approach has the great advantage that the ultimate resolution calibration can then be run on the very same fluorescent molecules that are to be employed in the actual experiment. Another version of the resolution calibration of a STED microscope as a function of the STED laser power is to use dot-like features, such as nuclear pores, stained with the same dye that is to be used in the actual experiment (Fig. 8.4), or other structures of dimensions much smaller than the diffraction limit such as single microtubule filaments [7]. Both of these sample types thus preclude any fluorophore-dependent effects that may originate from the consequence that the STED resolution depends on the saturation intensity, I_S, of the fluorescent dye used to label the sample (as shown in Eq. 8.1). The same STED power can thus provide a quite different STED effect depending on the dye, to the extreme situation in which the STED laser quickly photobleaches certain dyes such that no super-resolution effect can be obtained. This is because besides the absolute resolution provided by the instrument, a key parameter in STED microscopy (just like in conventional confocal microscopy) is also the signal-to-noise ratio (SNR) as a high-quality image requires sufficient contrast to resolve the signal above the noise of the background.

From the imaging of single sub-diffraction-limited beads or sub-diffraction-limited sized cellular structures, as shown in Figs. 8.3 and 8.4, it is possible to extract quantitatively the resolution of the STED microscope from measurements of the full width at half maximum (FWHM) of line intensity profiles across the objects of interest. This is most commonly done by fitting such intensity line profiles, $I(x)$, to a one-dimensional spatial Gaussian

$$I(x) = I_{\text{bkgd}} + I \exp\left[\frac{-(x - x_0)^2}{2\sigma^2}\right] \tag{8.2}$$

where I_{bkgd} is the intensity of the background fluorescence, I is the peak intensity, x_0 is the position of the peak, σ is the Gaussian width of the peak, and the FWHM is given by

$$\text{FWHM} = 2\sqrt{2\ln 2}\sigma. \tag{8.3}$$

An interesting alternative to these calibration measurements of sub-diffraction-limited beads and structures are also DNA origami-based GATTA-STED nanorulers consisting of two fluorescent marks of dense arrangements of multiple dye fluorophores at a specified distance of separation. Examples of confocal and STED images of such nanorulers specified to consist of two fluorescent marks separated by

Fig. 8.3 (continued) 775 nm STED laser, and time-gated detection ($0.5 \leq t_d \leq 7$ ns) with a spectral emission window of 603–666 nm. The STED laser power, projected pixel size, and FWHM results of the analysis of intensity line profiles are shown in Table 8.1. $N = 15$ for all analysis in Figures (**f**–**i**) for each image condition

Table 8.1 Image conditions and FWHM analysis results for all GATTA Beads in Fig. 8.3

Sample	STED laser power (mW; % of max available power)	Projected pixel size ($p_x = p_y$) (nm)	FWHM (mean ± standard deviation) (nm)
Bead R (Atto647N)	0	70	270 ± 12
	33 (10%)	39	140 ± 20
	82 (25%)	28	95 ± 9.4
	158 (50%)	21	73 ± 12
	291 (100%)	15	62 ± 9.7
Bead B (Oregon Green 488)	0	70	230 ± 13
	30 (10%)	44	110 ± 19
	77 (25%)	30	69 ± 14
	151 (50%)	22	56 ± 11
	300 (100%)	16	48 ± 14
Bead G (Atto 542)	0	70	260 ± 13
	27 (10%)	50	150 ± 18
	67 (25%)	35	110 ± 18
	131 (50%)	25	77 ± 13
	248 (100%)	18	61 ± 10
Bead O (Atto 594)	0	70	270 ± 31
	33 (10%)	36	160 ± 17
	82 (25%)	27	110 ± 15
	158 (50%)	20	75 ± 14
	291(100%)	15	59 ± 14

90 and 50 nm are shown in Fig. 8.5. By using these samples, it is in principle possible to directly determine the minimum STED laser power of the STED microscope that is required to resolve the two fluorescent marks as two separate structures by visual examination of a series of images acquired at different STED laser powers. Alternatively, for a full quantitative analysis, intensity line profiles across the two separate structures can be fit to the sum of two spatial Gaussians

$$I(x) = I_{\text{bkgd}} + I_1 \exp\left[\frac{-(x - x_{01})^2}{2\sigma^2}\right] + I_2 \exp\left[\frac{-(x - x_{02})^2}{2\sigma^2}\right] \tag{8.4}$$

where I_{bkgd} is the intensity of the background fluorescence, I_1 and I_2 are the respective peak intensities of each respective fluorescent mark, x_{01} and x_{02} are the respective positions of each peak, and σ is the Gaussian width of the peaks. From such fits, the FWHM is again given by Eq. (8.3), while the separation distance between the two fluorescent marks is given by

$$\text{Peak Separation} = |x_{01} - x_{02}| \pm \sqrt{2\sigma^2} \tag{8.5}$$

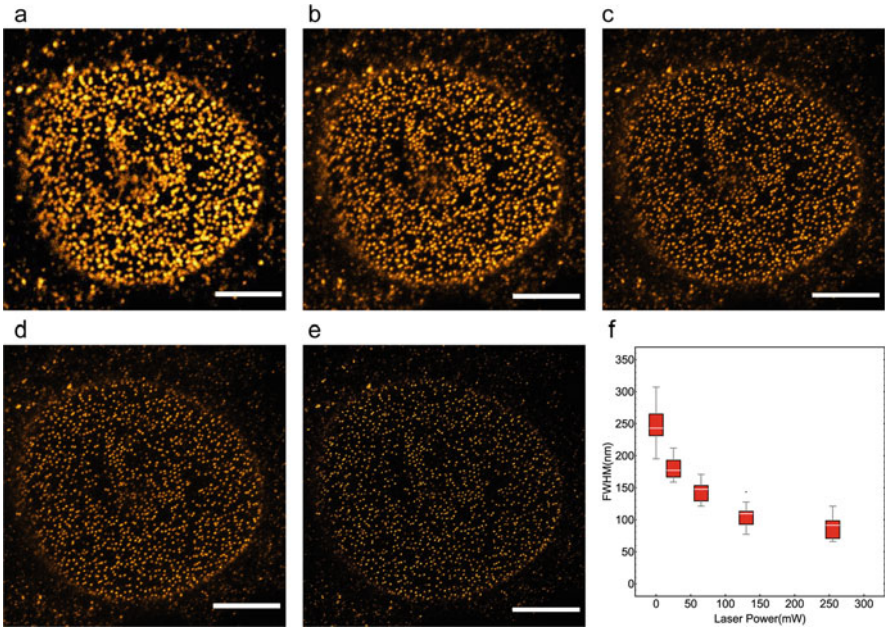

Fig. 8.4 Performance validation of STED microscope in 2D STED imaging mode with cells immunostained for nuclear pore complex protein Nup-153. (**a**–**e**) HeLa cells were fixed with paraformaldehyde, permeabilized with Triton X-100 (0.1%), blocked with bovine serum albumin (10%), and immunostained with primary antibody to Nup-153 (Abcam; ab24700; 1:500 dilution) and secondary goat anti-mouse IgG labeled with Alexa Fluor 532 (Thermo Fisher Scientific; A11002; 1:500 dilution), mounted in Prolong Gold mounting media, and imaged on a Leica STED 3X microscope with a STED white 100X 1.40 NA Plan APO oil immersion objective, 514 nm laser excitation, a continuous wave (CW) 660 nm STED laser, and time-gated detection ($1.5 \leq t_d \leq 6.5$ ns) with a spectral emission window of 550–624 nm. The STED laser power and projected pixel size ($p_x = p_y$) for each image was respectively (**a**) 0 mW and 74 nm, (**b**) 26 mW (10% of maximum available laser power) and 46 nm, (**c**) 65 mW (25%) and 32 nm, (**d**) 129 mW (50%) and 23 nm, and (**e**) 255 mW (100%) and 17 nm. The resolution of the resulting STED images was evaluated quantitatively as described in Fig. 8.3 by using the line profile tool in ImageJ (version 1.53j) to create line intensity profiles across select apparent single NUP complexes ($N = 15$ for each image condition). The full width-half maximum (FWHM) results of the intensity line profiles from this analysis are shown in traditional box-and-whisker plots in (**f**). The mean FWHM values ($\pm$ standard deviation) were respectively (**a**) 250 $\pm$ 32 nm, (**b**) 180 $\pm$ 16, (**c**) 140 $\pm$ 15 nm, (**d**) 110 $\pm$ 17 nm, and (**e**) 88 $\pm$ 17 nm. Scale bars = 5 μm

8.4.4 Time Alignment and Gating

STED microscopy can be implemented via pulsed or continuous (CW) laser sources. The classical implementation employs pulsed lasers both for the excitation and STED beam. A temporal misalignment of the excitation and STED beams will result in a confocal blurring around the STED image. Shifting the time synchronization of the STED laser with respect to the excitation laser will allow a perfect time alignment between the beams resulting in a well-contrasted super-resolution image. Over the

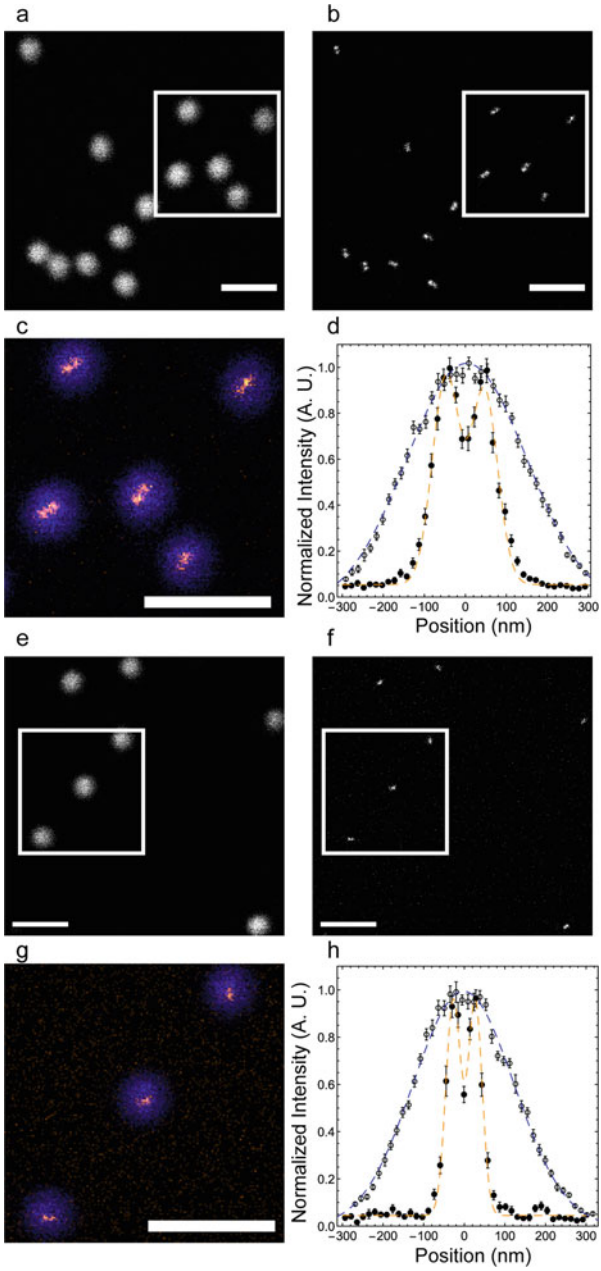

Fig. 8.5 Performance validation of STED microscope with GATTA-STED nanorulers (GattaQuant). Confocal, STED images, and image analysis thereof of GATTA-STED nanorulers consisting of two fluorescent marks of dense arrangements of the dye ATTO 647N that are separated by, respectively, (**a**–**d**) 90 nm (STED 90R) and (**e**–**h**) 50 nm (STED 50R). Images were acquired on a Leica STED 3X microscope with a STED white 100X 1.40 NA Plan APO oil immersion objective, 633 nm laser excitation, a pulsed 775 nm STED laser, and time-gated detection ($0.3 \leq t_d \leq 8$ ns) with a spectral emission window of 640–752 nm. The images were

years, a CW implementation has been favored over the pulsed one due to a reduced intensity of the STED beam delivered to the sample. In this case, a pulsed excitation laser is combined with a CW STED laser. In such an implementation, the confocal blurring will always appear and a time gating of the detected photons is needed as shown for the image examples in e.g. Figs. 8.3 and 8.4.

8.5 Application Examples

8.5.1 STED Imaging in Cells

STED microscopy is nowadays a well-known technique to disclose features and conduct co-localization studies at a nanoscale level. Here, we discuss the detailed procedure to acquire reliable multicolor STED images on a well-aligned and calibrated system.

The simplest multicolor STED imaging is done with dyes that have distinct excitation and preferably also distinct emission spectra but which can be depleted with a single STED laser. One of the best examples of such dye combinations are intermediate red dyes such as Alexa Fluor 594 or Atto 590 in combination with far red dyes such as Abberior Star Red or Abberior Star 635P (see example images in Fig. 8.6). Just as was the case for the STED images of the calibration samples shown in Figs. 8.3 and 8.4, it is also possible in these instances to tune the resolution by adjusting the STED laser power. One caveat, however, is that the SNR of the resulting images typically decreases with increasing STED laser power although one possibility in these instances is to use image deconvolution in order to enhance the contrast of such images as shown in Fig. 8.6b, h. A major advantage of this

Fig. 8.5 (continued) acquired in line scanning mode with a projected pixel size of $(15)^2$ nm^2 and with a STED laser power of respectively (**a**, **e**) 0 mW, (**b**) 82 mW (25%), and (**f**) 240 mW (80% of maximum available power). The resolution of the resulting STED images was evaluated quantitatively by using the line profile tool in ImageJ (version 1.53j) to create line intensity profiles across select apparent single nanorulers in the orientation of the two fluorescent marks as detected in the STED images ($N = 15$ for each image condition) and by fitting the resulting line intensity profiles for the confocal data to a one-dimensional spatial Gaussian, and the STED data to the linear sum of two one-dimensional spatial Gaussians (Wolfram Mathematica; version 12.0.0.0). (**a**, **e**) Confocal image data. (**b**, **f**) STED image data. (**c**, **g**) Magnified superimposed confocal (blue) and STED data (orange glow) of nanorulers from ROIs outlined by white squares in (**a**, **b**, **e**, and **f**). Scale bars = 1 μm. (**d**, **h**) Average (± standard error of the mean) of the intensity line profiles for (**d**) STED 90R and (**h**) STED 50R nanoruler image data from the confocal image data (open circles) and the STED image data (closed circles). Also shown in (**d**, **h**) are the best fits to the average confocal data (blue dashed line) and the average STED data (dashed orange line). The average FWHM (± standard deviation) of the confocal data for the STED 90R nanoruler was 326 ± 20 nm, while the average peak separation between the two distinct fluorescent marks in the STED data was 86 ± 20 nm. The average FWHM (± standard deviation) of the confocal data for the STED 50R nanoruler was 286 ± 22 nm, while the average peak separation between the two distinct fluorescent marks in the STED data was 54 ± 6 nm

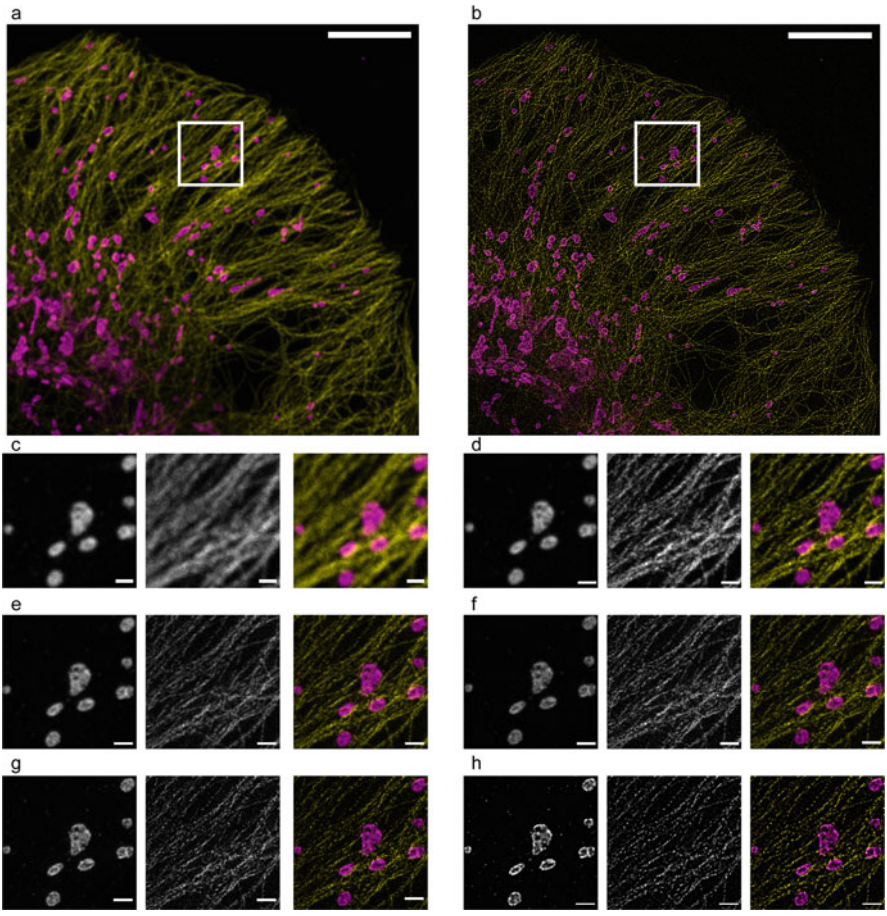

Fig. 8.6 Two-color STED image example in 2D STED imaging mode with a single pulsed 775 nm STED laser. (**a**–**h**) HeLa cells were fixed and stained as for image data in Fig. 8.3 except that immunostaining was done with primary antibodies to tyrosine tubulin (yellow; Sigma-Aldrich; T9028 (Clone TUB-1A2); monoclonal mouse IgG3; 1:500 dilution) and TOM20 (pink; Santa Cruz Biotechnology; sc-11,415; polyclonal rabbit IgG; 1:100 dilution) and secondary antibodies of respectively goat anti-mouse IgG labeled with Abberior Star Red (Abberior GmbH; STRED-1001; 1:500 dilution) and goat anti-rabbit IgG labeled with Atto 590 (Sigma-Aldrich; 68919; 1:500 dilution). Stained cells were imaged on a Leica STED 3X microscope with a STED white 100X 1.40 NA Plan APO oil immersion objective, in frame sequential mode with time-gated detection ($0.5 \leq t_d \leq 7$ ns), and respectively 561 nm (Atto 590) and 660 nm (Abberior Star Red) excitation and spectral emission windows of 589–643 nm (Atto 590) and 673–748 nm (Abberior Star Red). (**a**) Confocal image of tyrosine tubulin (yellow) and TOM20 (pink). The outlined ROI (white square) in (**a**) is shown in magnified view for (**c**) confocal image settings (left: TOM20; center: tyrosine-tubulin; right: overlay of TOM20 (pink) and tyrosine tubulin (yellow)); (**d**) 2D STED image with 775 nm STED laser power of 33 mW (10% of maximum STED laser power); (**e**) 2D STED image with 775 nm STED laser power of 82 mW (25%); (**f**) 2D STED image with 775 nm STED laser power of 158 mW (50%); and (**g**) 2D STED image with 775 nm STED laser power of 291 mW (100%). Also shown in (**b**, **h**) is the 2D STED image with 775 nm STED laser power of 291 mW (100%) after deconvolution using Huygens Professional at default settings for the Classical Maximum Likelihood Estimator algorithm (Scientific Volume Imaging). Scale bars in (**a**, **b**) are 10 μm, and (**c**–**h**) are 1 μm

approach to multicolor STED imaging is that in this instance there is no chromatic shift between the color channels. This is because in STED microscopy, it is the center of the STED PSF that determines the absolute alignment of the multicolor images [8]. This is in stark contrast to conventional confocal imaging where chromatic aberrations cannot be avoided. Thus, multicolor STED imaging with a single STED laser is an optimal arrangement for super-resolution co-localization studies as has been demonstrated previously [8]. Good practice, however, nevertheless always requires that single color control samples to optimize the detection channels for minimum cross talk, while it is also essential to acquire images at high SNR.

Multicolor STED microscopy is further possible with multiple STED and excitation beams (see example images in Fig. 8.7). But in cases of detailed co-localization studies, the chromatic aberration shift of the system in this instance must be evaluated by use of a calibration sample, usually a 100 nm diameter TetraSpeck bead sample. When the system is aligned the fluorescence emitted in the different spectral range should overlap both in confocal and STED modality. Furthermore, to avoid bleaching of the red-like dyes before their visualization, it is essential that the STED images are acquired starting with the most red-shifted fluorophore and ending with the most blue-shifted fluorophore. Additionally, if a 3D reconstruction of the sample is required, then the entire stack of images needs to be acquired channel by channel starting with the most red-shifted dye and ending with the most blue-shifted dye. Noteworthy here is that, due to the high intensity associated with the STED laser beam, photobleaching can also be a limiting factor in STED microscopy. Consequentially, it might be easy to acquire a single image of the sample at maximum STED power and resolution but much more challenging to acquire a z-stack of the same sample that will guarantee a 3D reconstruction of the region of interest. Depending on the needed resolution to disclose the required features of a study, the employed STED power might therefore be reduced following the resolution calibration. When a multicolor STED image is required for a certain experiment, the scientist would further need to decide for example if the images should provide the same resolution per each fluorescent dye or if it is acceptable to acquire the images at the maximum achievable resolution per each dye. The system needs to be calibrated and the STED power must be tuned accordingly. Depending on the analysis that is run on the acquired images, one solution might be favorable to the other.

8.5.2 STED Imaging in Deep Tissue

The very principle that STED imaging is based upon makes it unfortunately susceptible to light aberrations and scattering that occur with increasing depth in thicker samples. Yet a precise spatial and temporal overlap of the excitation and STED depletion laser beams is required to obtain the narrow excitation focus as explained in this chapter. Thus, light scattering as induced by thick or optically dense samples reduces the ability to optimize the beam shape used for the STED depletion beam. The deeper within or the denser a sample is, the lower the STED efficiency and

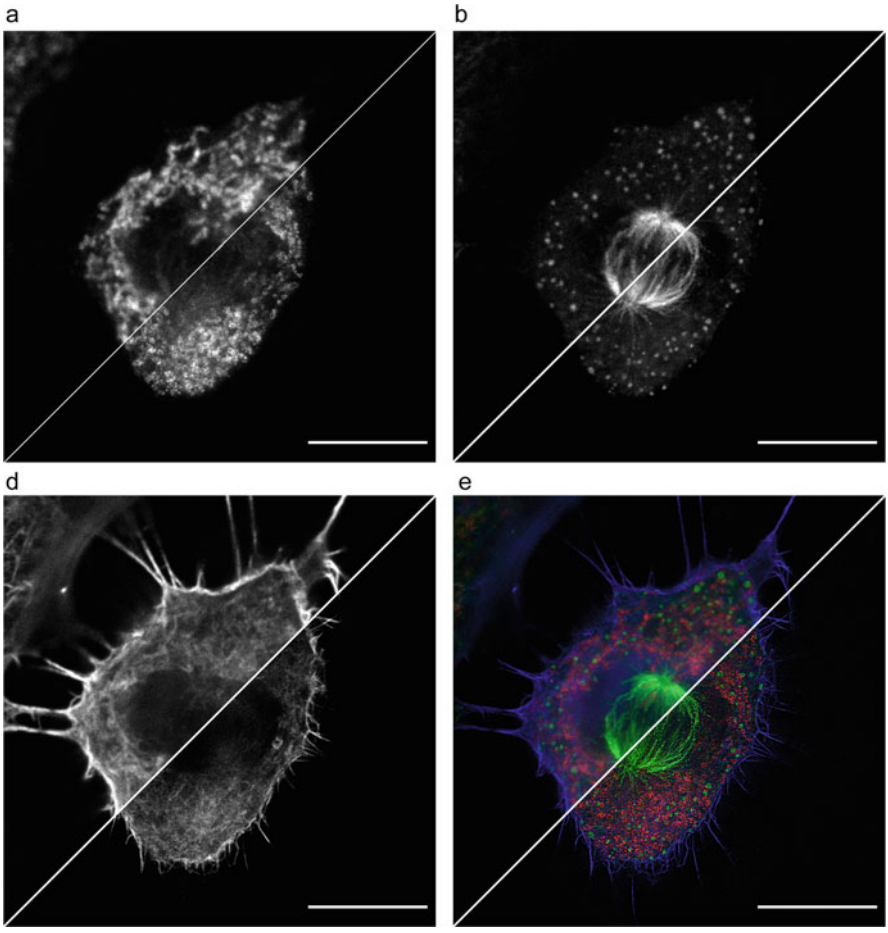

Fig. 8.7 Comparison of three-color confocal (top left of each image) and 2D STED images (bottom right of each image). (**a**) Mitochondria stained as described for data in Fig. 8.3 but with primary antibody to TOM20 (Santa Cruz Biotechnology;sc-11415; polyclonal rabbit IgG; 1:100 dilution) and secondary antibody labeled with Abberior Star 635P (Abberior GmbH; ST635P-1002; 1:500 dilution). (**b**) Tyrosine-Tubulin stained with primary antibody (Sigma-Aldrich; T9028 (Clone TUB-1A2); monoclonal mouse IgG3; 1:500 dilution) and secondary antibody labeled with Alexa 555 (Thermo Fisher Scientific; A32727; 1:500 dilution). (**c**) F-actin stained with phalloidin labeled with Oregon Green 488 (Thermo Fisher Scientific; O7466; 1 unit per coverslip). (**d**) Superimposed three-color images of mitochondria (red), tyrosine tubulin (green) and F-actin (blue). Stained cells were imaged on a Leica STED 3X microscope with a STED white 100X 1.40 NA Plan APO oil immersion objective with a projected pixel size of 30 nm, in frame sequential mode in the following order: (1) Abberior Star Red emission channel (**a** excitation at 633 nm; STED depletion at 775 nm at STED laser power of 82 mW (25%); spectral emission window of 656–737 nm; time-gated detection of $0.5 \leq t_d \leq 7$ ns), (2) Alexa Fluor 555 emission channel (**b** excitation at 561 nm; STED depletion at 660 nm at STED laser power of 67 mW (25%); spectral emission window of 566–613 nm; time-gated detection of $1 \leq t_d \leq 8.5$ ns), and (3) Oregon Green emission channel (**c** excitation at 488 nm; STED depletion at 592 nm at STED laser power of 77 mW (25%); spectral emission window of 494–549 nm; time-gated detection of $1.5 \leq t_d \leq 6.5$ ns). Scale bars = 10 μm

therefore the higher the STED power requirements to obtain any super-resolution images. In addition, the often weaker signal requires longer acquisition times and leads to increased photobleaching and a higher signal-to-noise level. These limitations mean that albeit it is possible, STED imaging is much more challenging in thicker or optically denser samples when compared to thin samples close to the cover glass. The achievable light penetration depth and resolution depends on the optical properties of the sample, but for each, there is ultimately a limit at which STED imaging may not yield higher resolution images, then airy-scan imaging, conventional confocal imaging, and ultimately multi-photon imaging.

At present most super-resolution studies have been imaging samples of up to 10 μm thickness (see review: [9]), which is a standard tissue section thickness, but in a biological context is not considered deep tissue imaging. Although STED imaging of bright and very photostable fluorescent beads has been demonstrated as deep as 155 μm [10], most biological samples have more light scattering properties throughout the tissue and have fluorescence less bright and less photostable than such optimal bead standard samples. Nevertheless, various studies have demonstrated the usability and superior imaging resolution of STED in common thick biological specimen such as in several hundred micrometer thick brain slices (for protocol: [11]) or actin filament dynamics in live mouse brains up to 40 μm away from the implanted cranial cover glass window [12, 13]. Willig and Nägerl [11] have been able to visualize via STED time-lapse imaging the dynamics of dendritic spines of pyramidal neurons in living hippocampal mouse brain slices with a resolution of ~100 nm. Since the STED microscope setup is very similar to conventional laser scanning confocal and multi-photon microscopy, similar sample approaches (e.g., upright microscopes, sample mounting, objective types) and limitations (e.g., sample movement due to growth or drift, sample optical density, and viability issues) apply.

To increase the axial resolution (z dimension) in 3D stacks of samples, adaptive optics (AO) are being developed for STED [14, 15]. To achieve a higher axial resolution, multiple laser beams need to be shaped independently, so that the point-spread function is narrowed along the axial dimension. The additional beam shaping elements make maintaining the beam alignments in 3D STED even more difficult than in 2D STED with increasing aberration at increased sample depth [16]. Another approach to improve STED imaging in thicker samples is to use two-photon (2P) STED [17–19] to compensate for the changing and increasing light scattering along the z-axis of the sample. 2P STED can improve the spatial resolution achieved by regular two-photon microscopy (two to sixfold) at moderate imaging depths [17].

Taken together, STED imaging in deeper areas of biological samples in vivo and ex vivo is achievable, but requires considerately more effort to test and establish compared to conventional STED imaging with samples very close to the cover glass. It is therefore advisable for anyone interested in deep tissue STED imaging to seek out established users of the technique to learn and troubleshoot the methodology and potentially test out any envisaged sample.

Take-Home Message

The super-resolution effect in STED microscopy is obtained by the combination of stimulated emission depletion (STED) laser beam, which overlaps in space and time with a standard confocal excitation beam, and which has been engineered to specifically deplete all excited fluorophores at the periphery of a local zero (by the process of stimulated emission) while all fluorophores at the center of the local zero of the STED beam are permitted to relax by conventional spontaneous emission, thus resulting in a much improved effective emission PSF (schematic in Fig. 8.1c and image examples in Figs. 8.3, 8.4, 8.5, 8.6, and 8.7).

STED microscopy has become a mature super-resolution microscopy technique that is routinely applied for single- and multicolor imaging in thinner specimen (<10 µm) such as fixed cells. As with any advanced technique however it is essential to fully validate the performance of the STED microscope prior to imaging of the specimen of interest. This chapter introduces a range of such calibration samples and shows representative data that should be obtainable on a well-aligned system. Much work is also currently being done on improving the performance and usability of STED microscopy in thicker tissue samples.

References

1. Hell SW, Wichmann J. Breaking the diffraction resolution limit by stimulated emission: stimulated-emission-depletion fluorescence microscopy. Opt Lett. 1994;19(11):780–2. https://doi.org/10.1364/ol.19.000780.
2. Klar TA, Jakobs S, Dyba M, Egner A, Hell SW. Fluorescence microscopy with diffraction resolution barrier broken by stimulated emission. Proc Natl Acad Sci U S A. 2000;97(15):8206–10. https://doi.org/10.1073/pnas.97.15.8206.
3. Eggeling C, Ringemann C, Medda R, Schwarzmann G, Sandhoff K, Polyakova S, et al. Direct observation of the nanoscale dynamics of membrane lipids in a living cell. Nature. 2009;457(7233):1159–62. https://doi.org/10.1038/nature07596.
4. Kastrup L, Blom H, Eggeling C, Hell SW. Fluorescence fluctuation spectroscopy in subdiffraction focal volumes. Phys Rev Lett. 2005;94(17):178104. https://doi.org/10.1103/PhysRevLett.94.178104.
5. Sezgin E, Schneider F, Galiani S, Urbančič I, Waithe D, Lagerholm BC, Eggeling C. Measuring nanoscale diffusion dynamics in cellular membranes with super-resolution STED–FCS. Nat Protoc. 2019;14(4):1054–83. https://doi.org/10.1038/s41596-019-0127-9.
6. Tang J, Ren J, Han KY. Fluorescence imaging with tailored light. Nanophotonics. 2019;8(12):2111–28. https://doi.org/10.1515/nanoph-2019-0227.
7. Wegel E, Gohler A, Lagerholm BC, Wainman A, Uphoff S, Kaufmann R, Dobbie IM. Imaging cellular structures in super-resolution with SIM, STED and localisation microscopy: a practical comparison. Sci Rep. 2016;6:27290. https://doi.org/10.1038/srep27290.
8. Galiani S, Waithe D, Reglinski K, Cruz-Zaragoza LD, Garcia E, Clausen MP, et al. Super-resolution microscopy reveals compartmentalization of peroxisomal membrane proteins. J Biol Chem. 2016;291(33):16948–62. https://doi.org/10.1074/jbc.M116.734038.
9. Liu W, Toussaint KC Jr, Okoro C, Zhu D, Chen Y, Kuang C, Liu X. Breaking the axial diffraction limit: a guide to axial super-resolution fluorescence microscopy. Laser Photonics Rev. 2018;12(8):1700333. https://doi.org/10.1002/lpor.201700333.

10. Yu W, Ji Z, Dong D, Yang X, Xiao Y, Gong Q, et al. Super-resolution deep imaging with hollow Bessel beam STED microscopy. Laser Photonics Rev. 2016;10(1):147–52. https://doi.org/10.1002/lpor.201500151.
11. Willig KI, Nägerl UV. Stimulated emission depletion (STED) imaging of dendritic spines in living hippocampal slices. Cold Spring Harb Protoc. 2012;2012(5):pdb.prot069260. https://doi.org/10.1101/pdb.prot069260.
12. Willig KI, Steffens H, Gregor C, Herholt A, Rossner MJ, Hell SW. Nanoscopy of filamentous actin in cortical dendrites of a living mouse. Biophys J. 2014;106(1):L01–3. https://doi.org/10.1016/j.bpj.2013.11.1119.
13. Urban NT, Willig KI, Hell SW, Nägerl UV. STED nanoscopy of actin dynamics in synapses deep inside living brain slices. Biophys J. 2011;101(5):1277–84.
14. Gould TJ, Burke D, Bewersdorf J, Booth MJ. Adaptive optics enables 3D STED microscopy in aberrating specimens. Opt Express. 2012;20(19):20998–1009. https://doi.org/10.1364/OE.20.020998.
15. Osseforth C, Moffitt JR, Schermelleh L, Michaelis J. Simultaneous dual-color 3D STED microscopy. Opt Exp. 2014;22(6):7028–39. https://doi.org/10.1364/OE.22.007028.
16. Patton BR, Burke D, Owald D, Gould TJ, Bewersdorf J, Booth MJ. Three-dimensional STED microscopy of aberrating tissue using dual adaptive optics. Opt Express. 2016;24(8):8862–76. https://doi.org/10.1364/OE.24.008862.
17. Bethge P, Chereau R, Avignone E, Marsicano G, Nagerl UV. Two-photon excitation STED microscopy in two colors in acute brain slices. Biophys J. 2013;104(4):778–85. https://doi.org/10.1016/j.bpj.2012.12.054.
18. Moneron G, Hell SW. Two-photon excitation STED microscopy. Opt Express. 2009;17(17):14567–73. https://doi.org/10.1364/oe.17.014567.
19. Ter Veer MJT, Pfeiffer T, Nagerl UV. Two-photon STED microscopy for nanoscale imaging of neural morphology in vivo. Methods Mol Biol. 2017;1663:45–64. https://doi.org/10.1007/978-1-4939-7265-4_5.